05,11

Temperature-baric features of magnetic characteristics in systems with structural transitions of the displacement type

© V.I. Valkov[1], A.V. Golovchan[1], I.F. Gribanov[1], B.M. Todris[1], E.P. Andreychenko[1], V.I. Mitsiuk[2], A.V. Mashirov[3]

[1] Galkin Donetsk Institute for Physics and Engineering, Donetsk, DNR, Russia
[2] Scientific and Practical Materials Research Center, National Academy of Sciences of Belarus, Minsk, Belarus
[3] Kotelnikov Institute of Radio Engineering and Electronics, Russian Academy of Sciences, Moscow, Russia

E-mail: valkov09@gmail.com

Received November 8, 2022
Revised November 8, 2022
Accepted November 16, 2022

Using pnictides MnAs and germaindes $Mn_{0.89}Cr_{0.11}NiGe$ as an example, the transformation of thermobaric features of their magnetic characteristics at high pressures is considered. A unified approach is used to describe paramagnetic (PM) structural transitions of the displacement type with a change in the symmetry $PM(P6_3/mmc)-PM(Pnma)$ from hexagonal to orthorhombic. It is shown that the competition between the parameters of the structural and magnetic orders in both systems manifests itself differently in the stabilization and alternation of the so-called high-spin and low-spin magnetically ordered states initiated by pressure. As a consequence, the structural contribution in these systems weakens (MnAs) or enhances $Mn_{0.89}Cr_{0.11}NiGe$ the giant magnetocaloric effect in the temperature-baric region of the first-order magnetostructural phase transitions.

Keywords: structural phase transitions of the displacement type, magnetostructural phase transitions, helimagnetism, ferromagnetism, high spin-low spin states, direct magnetocaloric effect.

DOI: 10.21883/PSS.2023.02.55412.523

1. Introduction

In some pnictides $Mn_{1-y}A_yAs$ (A — Fe, Co, Ni) [1–4] and germanides $Mn_{1-x}B_xNiGe$ (B — Cr, Fe), $Co_{1-x}Cu_xMnGe$ [5–10], magnetic ordering is preceded in temperature by displacement-type structural transitions from hexagonal paramagnetic phase ($P6_3/mmc$ symmetry group) to orthorhombic paramagnetic phase ($Pnma$ symmetry group). These structural transitions $PM(P6_3/mmc)-PM(Pnma)$ in both system classes are accompanied with specific abnormal temperature dependence of inverse paramagnetic susceptibility $\chi^{-1}(T)$ associated with subsequent features of magnetic order occurrence. Magnetic order occurring at temperatures $T_C(T_N)$ that are considerably lower than structural paramagnetic transition T_t is primarily caused by spin polarization of Mn d-electrons. The degree of spin polarization in pnictides depends on pressure and lattice symmetry. In pressure $0 \le P \le 40$ kbar range, distinction is made between: „high-spin" $HS(P6_3/mmc)$ $B8_1$ and „low-spin" $LS(Pnma)$ B31 phases of MnAs [11,12]. Generally, magnetic order stabilization in both system classes causes a magnetocaloric effect enhanced by phase transition [13,14]. Abnormal dependences $\chi^{-1}(T)$ in pnictides $Mn_{1-y}A_yAs$ and germaindes $Mn_{1-x}B_xNiGe$ differ significantly because structural transitions $PM(P6_3/mmc)-PM(Pnma)$ similar in symmetry-group characteristics are different in the type of implementation. In pnictides — these are second order phase transitions caused by smooth growth of optical displacements of As atoms, and in germaindes — these are first order phase transitions accompanied with emergent optical displacements of Ni and Ge atoms and with change in a lattice cell volume. In this case, local displacements of As, Ni and Ge for the given cell incur specific displacements of Mn atoms and, thus, duplication of a lattice cell as a whole [15]. In addition, orthorhombic phase is supported by magnetic order in pnictides and germanides in a different way. In MnAs and MnAs-based alloys, appearance of ferromagnetism (FM) comes with orthorhombic symmetry disappearance and hexagonal symmetry stabilization. This process is implemented as 1st order magnetostructural phase transition $PM(Pnma)-FM(P6_3/mmc)$. In germanides, on the other hand, magnetic order of (soft helimagnetic structure (HM)) is supported by orthorhombic symmetry and implemented as 2nd order isostructural transition $PM(Pnma)-HM(Pnma)$. These processes are consistent with abnormal behavior of $\chi^{-1}(T)$ dependences for system classes, see Figure 1.

Another set of features occurs under hydrostatic pressure exposure. In pnictides, hexagonal phase $FM(P6_3/mmc)$ that may exist up to $P \le 4.5$ kbar is designated as „high-spin" (HS) phase with saturation magnetic moment $3.4\mu_B$. At high pressures, no 1st order magnetostructural transition $PM(Pnma)-FM(P6_3/mmc)$ and, therefore, high-spin

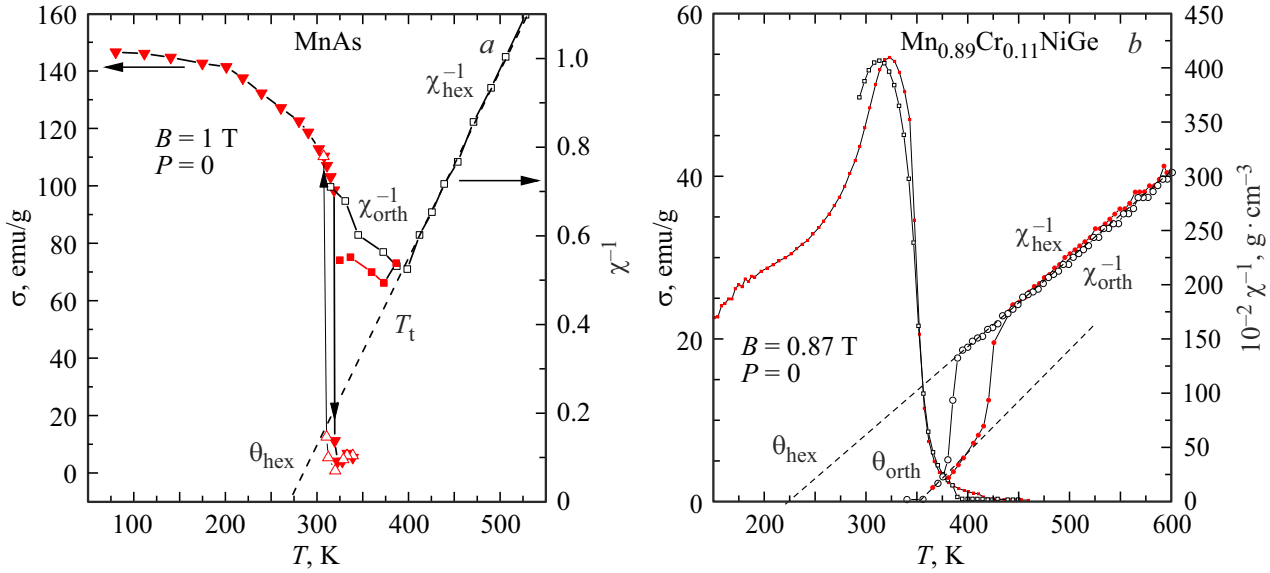

Figure 1. Typical temperature dependences of magnetization σ and inverse susceptibility χ^{-1} of pnictide (MnAs) and germanide ($Mn_{0.89}Cr_{0.11}NiGe$) samples [6].

state (HS) with hexagonal crystalline lattice are observed. In this case, according to $P-T$ phase diagram of MnAs and MnAs-based alloys [1,14], low-temperature orthorhombic phase ($Pnma$) is implemented as a low-spin magnetic structure [1]. At pressures above 4.5 kbar, noncollinear low-spin states with orthorhombic crystalline structure LS($Pnma$) are stabilized. Magnetization dependences $\sigma(T)$ in Figure 2, *a* in field 10 kOe give an idea of low-spin (LS) nominally ferromagnetic state FM($Pnma$), where $\sigma(T)$ is not higher than 1 μ_B ($\sigma = 44$ emu/g), Figure 2, *a*. For comparison, with $P = 0$, high-spin (HS) ferromagnetic FM($P6_3/mmc$) state in this field has magnetization $\sigma = 140$ emu/g ($\mu = 3.4\,\mu_B$), Figure 1. Neutron diffraction measurements also confirm that magnetic moment μ in low-temperature magnetic-ordered orthorhombic states [11,12] is reduced. Pressure increase generally leads to separation of structural transition T_t and magnetic transition $T_{N,C}$ temperatures from each other. And low-spin magnetic order appearance processes are always preceded with specific abnormal behavior or inverse paramagnetic susceptibility χ^{-1}, Figure 2, *b*.

In $Mn_{1-x}Cr_xNiGe$ system germanides, on the other hand, pressure exposure brings together and finally brings into coincidence the structural and magnetic transition temperatures. This results in transformation of 2nd order isostructural transition PM($Pnma$)−HM($Pnma$) into 1th order magnetostructural transition PM($P6_3/mmc$) → HM($Pnma$) [9]. In this case, abnormal splitting of dependence $\chi^{-1}(T)$ in Figure 1, *b* specific to samples with isostructural transitions PM($Pnma$)−HM($Pnma$) disappears.

The main purpose of this study is to describe and perform theoretical analysis of magnetostructural state transformation of systems under magnetic field and pressure exposure in both system classes within a single structural transition model PM($P6_3/mmc$) ↔ PM($Pnma$).

2. Underlying assumptions for phenomenological description of magnetostructural transitions in the pnictides and germanides of interest

In this section, we rely on the provisions of [16,17] with the main of them limited to the following assumptions.

1. Separation between spin and crystalline subsystems is introduced.

2. Displacement-type structural transition is described on the basis of so called local soft mode that describes group optical displacement of As atom in MnAs and Ni atom in $Mn_{1-x}Co_xNiGe$ in classical approximation [18–21]. Statistical averages of these displacements $\langle Q_n \rangle$ define the structural order parameter $\langle Q_n \rangle = Q_0$. Competition between intracell $V(Q_n)$ and intercell $\frac{1}{2}\sum_{nn'} v Q_n Q_{n'}$ couplings defines characteristic temperatures T_t of structural transition and is the cause of temperature dependence of mode oscillation frequency undergoing „freezing“ below T_t. Dependence of intercell couplings $\sum v = v_0(e_1, e_2) = v_0(1 + L_2 e_1 + L_3 e_2)$ on volume strain $e_1 = (e_{xx} + e_{yy} + e_{zz})$ and orthorhombic distortions $e_2 = (e_{xx} - e_{yy})/\sqrt{3}$ of the lattice is defined by baric properties ($T_t(P)$) and the kind of structural transition.

3. Spin subsystem properties in the systems of interest are defined by interacting collective *d*-electrons. Within the Hubbard model, the average spin on point $\langle S_i \rangle$, type of magnetic structure and magnetic disordering temperatures $T_{C,N}$ depend on the occupation of magnetoactive *d*-zone *n* and relationship between intraatomic exchange integrals *J*

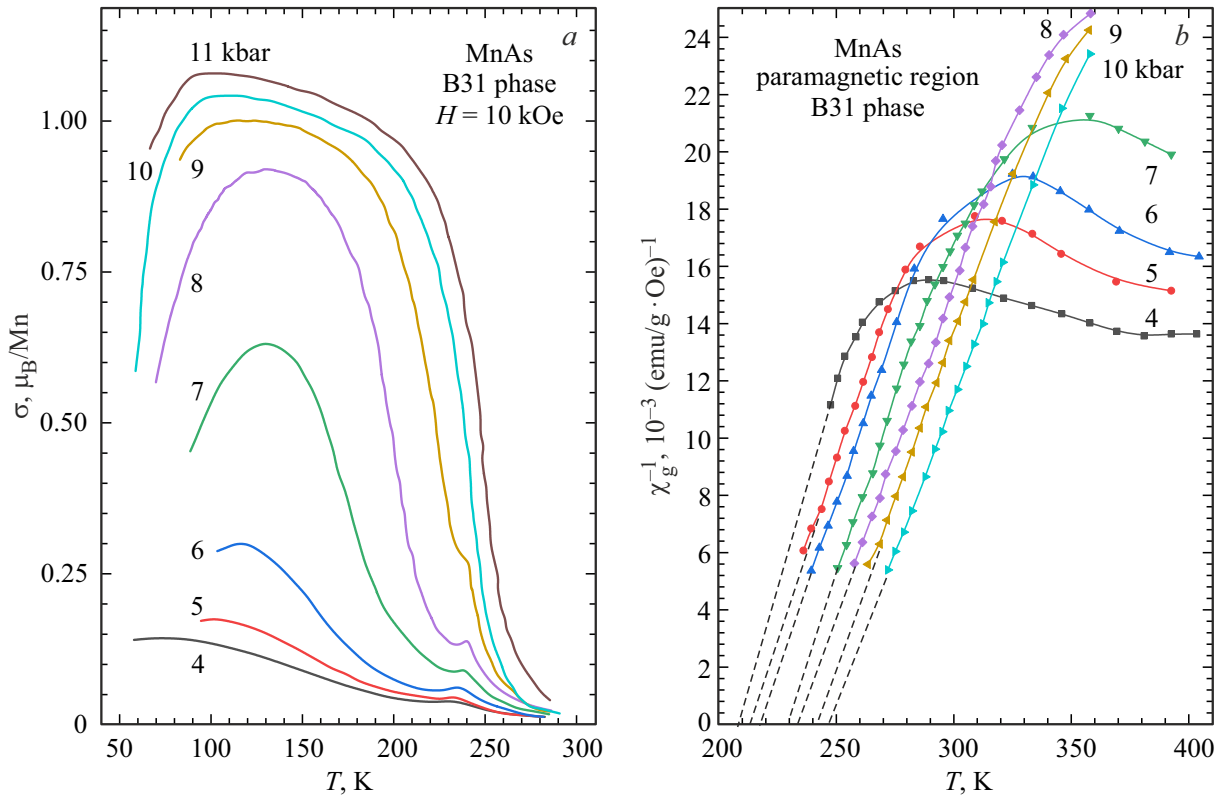

Figure 2. Baric features of thermomagnetic dependences for Mn (a) atom and inverse paramagnetic susceptibility of (b) MnAs in low-spin orthorhombic state [1].

and interatomic transfer integrals of d-electrons $t_{ij}(e_1, Q_0)$. However, inability to use molecular field approximations for adequate description of magnetic disordering of itinerant electrons makes the theoretical analysis of magnetostructural phase transitions in these systems very difficult. To bypass these difficulties, approaches are often used in which, in order to describe spin system properties, interelectronic interactions are limited to only Heisenberg-type spin-spin couplings $-\sum_{nk,n'k'} J^{kk'}_{nn'}\hat{s}^k_n\hat{s}^{k'}_{n'}$ by calculating effective interatomic integrals $J^{kk'}_{nn'} \equiv J^{kk}_{nn'}(e_1, Q_0)$. However, such approach does not provide different saturation magnetization $M^s = 2\mu_B|\langle\hat{s}^{k'}_{n'}\rangle|$ proportional to statistical average $\langle\hat{s}^{k'}_{n'}\rangle$ — for hexagonal phase ($e_{1\text{hex}}$, $Q_0 = 0$) and orthorhombic phase ($e_{1\text{orth}}$, $|Q_0| > 0$). Since when $T = 0|\langle\hat{s}^k_{n'}\rangle| = s$, $J^{kk'}_{nn'} \equiv J^{kk'}_{nn'}(e_1, Q_0)$ with any form of dependence. Therefore, to take into account the change in saturation magnetization when the type of magnetostructural state or pressure changes, an additional parameter — orthogonal space-periodic field — is introduced in the Hamiltonian-type spin Hamiltonian

$$\mathbf{O}^k_n = O[\sin(\mathbf{qR}^k_n), -\cos(\mathbf{qR}^k_n), 0], \quad (\mathbf{O}^k_n\mathbf{h}^k_n) = 0,$$

which acts on the spin component orthogonal to the quantization axis

$$\mathbf{h}^k_n = h\mathbf{u}^k_n = h[\cos(\mathbf{qR}^k_n)\sin(\vartheta), \sin(\mathbf{qR}^k_n)\sin(\vartheta), \cos(\vartheta)]$$

of helimagnetic structure with wave vector $\mathbf{q}[0, 0, q_a]$ in magnetic field $H_0 = [0, 0, H_0]$. Competition between Fourier components of exchange integrals

$$J(\mathbf{q}) = \sum_{k,n} J^{kk'}_{nn'}(q_a, Q^2_0, e_1) \equiv J(q_a)$$

and $|\mathbf{O}^k_n| \equiv O(Q^2_0)$ controls $T_{C,N}$ and the measured saturation magnetization with the specified eigenvalue s of spin operator of $\hat{s}^k_n$ k-th atom of Mn in n-th cell that was initially chosen for the system being described [16,17]. This competition to some degree simulates the competition between J and t_{ij} in the itinerant electrons system. For simplicity, it is also believed that only Mn atoms are magnetoactive, antiferromagnetic state for pnictides and germanides corresponds to helimagnetic structure (HM) with wave vector $\mathbf{q}[0, 0, q_a]$ and is only stabilized in orthorhombic phase (condition (9)). Full free energy potential of magnetostructural system is addressed as a sum of potentials of spin subsystem Ω_S and structural-elastic subsystem $\Omega_Q + \Omega_e$: $\Omega = \Omega_S + \Omega_Q + \Omega_e$. Ω_S, Ω_Q are calculated within single-particle approaches: in two-component space-periodic filed approximation $\mathbf{\Delta}^k_n = \mathbf{h}^k_n + \mathbf{O}^k_n \equiv \mathbf{V}^k_n|h^k_n + O^k_n| = \mathbf{V}^k_n\sqrt{h^2 + O^2}$ for a spin subsystem with helimagnetic order (HM) [16] and in displaced harmonic oscillator approximation (dso) [22] for a structural subsystem undergoing transition $(\text{hex}, P6_3/mmc) \leftrightarrow (\text{orth}, Pnma)$ with applicable

parameters which define the type of system. These parameters include combinations of coefficients of the thermodynamic potential, which form baric dependences of structural and magnetic transition temperatures, their behaviors (1th or 2nd order), initial types of magnetic structures and appropriate effective initial magnetic moments $\mu = 2\mu_B s$ of Mn atoms.

The purpose of the study — description of magnetostructural system state transformation under magnetic field and pressure exposure in both system classes — is achieved by solution of equations of state $\partial\Omega/\partial Q_0 = 0$ (1a), $\partial\Omega/y = 0$ (1b), which are reduced to a common form for pnictides and germanides.

3. Equations of state and their solutions

$$\partial\Omega_s/\partial Q_0 + \partial\Omega_{Q\mathrm{dso}}/\partial Q_0 = 0, \tag{1a}$$

$$y = B_s(X)\frac{h}{\sqrt{(hs)^2 + s^2O^2}}, \tag{1b}$$

$$h \equiv h(y) = 2\big[J(q_a)\big(\sin(\vartheta)^2\big) + J(0)\big(\cos(\vartheta)^2\big)\big]sy + 2\mu_0 H_0\cos(\vartheta), \tag{2}$$

where Brillouin function

$$B_s(X) = \left(\frac{1}{2s+1}\right)\coth\frac{1}{2s+1}X - \left(\frac{1}{2s}\right)\coth\frac{1}{2s}X;$$

ϑ — angle between h_n^k and H_0;

$$X = \frac{1}{k_B T}\sqrt{(hs)^2 + O^2s^2},$$

$$J(q_a) = \sum_{\Delta R} J(|\Delta\mathbf{R}|)\cos(\mathbf{q}\Delta\mathbf{R}) \approx J_0(Q_0^2, e_1) + J_1(Q_0^2, e_1)\cos(\Psi) + J_2(Q_0^2, e_1)\cos(2\Psi), \tag{3a}$$

$$J_i(Q_0^2, e_1) = \lambda_{ih}e_1 + \lambda_i Q_0^2 + \lambda_{1i}e_1Q_0^2 + \lambda_4 Q_0^4 + \lambda_6 Q_0^6, \tag{3b}$$

$\Psi = q_a c_{\mathrm{hex}}/2$, $2\Psi = q_a c_{\mathrm{hex}}$; c_{hex} — hexagonal lattice parameters along axis $0z$, structural order parameter $Q_0 = \langle Q_n\rangle_{\mathrm{dso}}$ and magnetic order parameter

$$\langle\hat{m}_n^k\rangle = \langle\mathbf{u}_n^k\hat{\mathbf{s}}_n^k\rangle \equiv m = \frac{h}{\sqrt{(hs)^2 + O^2s^2}}M = ys$$

are formally defined by expressions (4), (5) [16]. For calculation, use distribution function $\rho_{\mathrm{dso}}(Q_n)$ in displaced harmonic oscillator (6a) and density matrix ρ_n^k in mean field approximation (6b),

$$\langle Q_n\rangle_{\mathrm{dso}} = \int_{-\infty}^{\infty}\rho_{\mathrm{dso}}(Q_n)Q_n dQ_n, \tag{4a}$$

$$\sigma = \langle[Q_n - Q_0]^2\rangle_{\mathrm{dso}}, \tag{4b}$$

$$M = \mathrm{Sp}\{\hat{M}_n^k\rho_n^k(\hat{M}_n^k)\}, \tag{5}$$

$$\rho_{\mathrm{dso}}(Q_n) = \frac{1}{\sqrt{2\pi\sigma}}\exp\left[\frac{-(Q_n - Q_0)^2}{2\sigma}\right], \tag{6a}$$

$$\rho_n^k(\hat{M}_n^k) \equiv \rho_n^k = \frac{e^{\beta|h_n^k + O_n^k|\mathbf{V}_n^k\hat{\mathbf{s}}_n^k}}{z(X)} = \frac{e^{\beta\sqrt{h^2+O^2}\hat{M}_n^k}}{z(X)}, \tag{6b}$$

$$z(X) = \mathrm{Sp}\,e^{\beta(\sqrt{h^2+O^2})\hat{M}_n^k} \equiv \sum_{M_n^k=-s}^{s} e^{\beta(\sqrt{h^2+O^2})M_n^k} = \mathrm{sh}[(1 + (2s)^{-1})X]/\,\mathrm{sh}[(2s)^{-1}X]. \tag{6c}$$

Here, helimagnetic structure existing conditions at $\mathbf{H}_0 = 0$ and $H_0 = [0, 0, H_0] > 0$ are as follows, respectively,

$$\cos\Psi = \begin{cases}\delta(Q_0), & \text{at } |\delta(Q_0)| < 1,\\ 1, & \text{otherwise,}\end{cases} \tag{7}$$

$$\cos\vartheta = \begin{cases}\frac{2H_0\mu_B}{(J(q_a)-J(0))y} & \text{at } |\delta(Q_0)| < 1,\\ & 0 < \frac{2H_0\mu_B}{(J(q_a)-J(0))y} < 1,\\ 1, & \text{otherwise,}\end{cases} \tag{8}$$

$$\delta(Q_0) = J_1(Q_0, e_1)/4|J_2(Q_0, e_1)| = 1 - AQ_0^2 + BQ_0^4. \tag{9}$$

3.1. MnAs

Equations (1) are easily reduced to the description of the appropriate systems of interest. The applicable parameters for MnAs are defined by such selection of dependences $v_0(e_1, e_2)$ and $J\big(q_a(Q_0^2, e_1)\big)$ that ensure consistency between calculation results and experimental data at atmospheric pressure such as saturation magnetization of high-spin phase FM($P6_3/mmc$) $\sigma_{\mathrm{hex}} \approx 140$ emu/g,

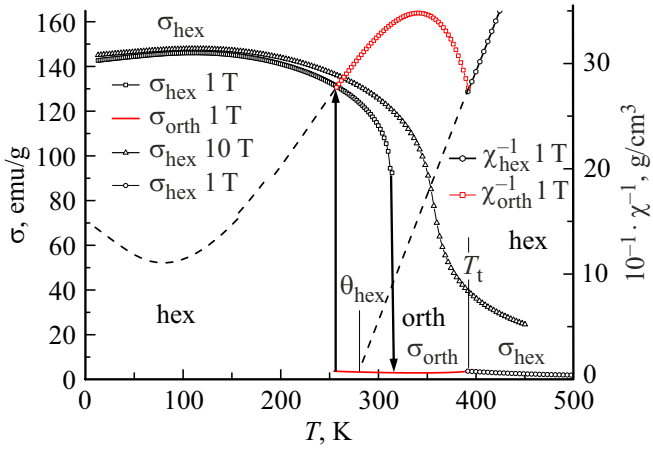

Figure 3. Magnetostructural transition transformation in MnAs with change in magnetic field induction. ↓ — lability temperature for FM(hex)−T_{C2} phase; ↑ — corresponds to (T_{C1}) calculated from equality of thermodynamic potentials of FM(hex) and PM(orth) phases. Inductions $B = \mu_0 H_0$ ($\mu_0 = 1$) are shown for the curves.

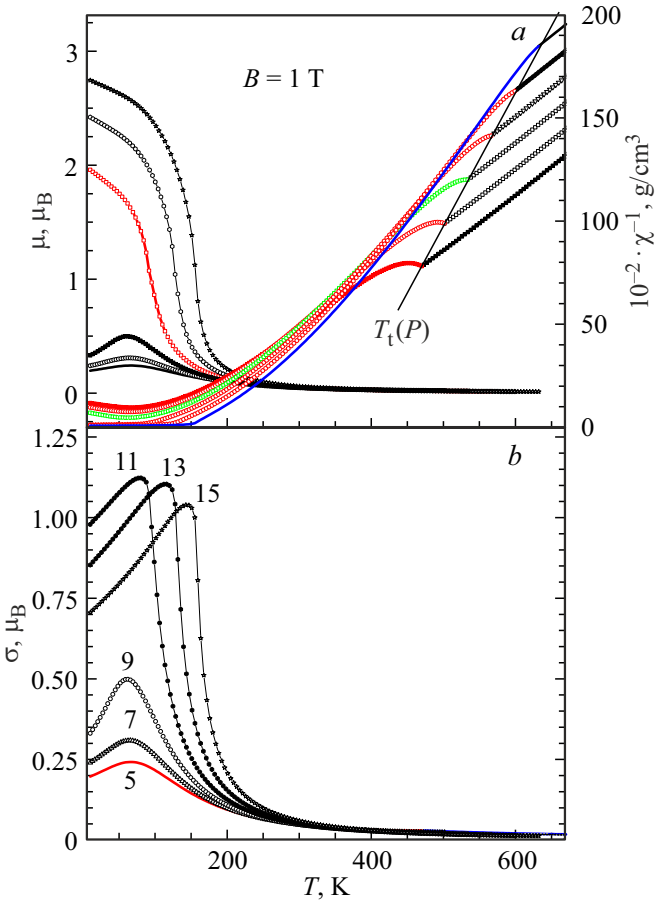

Figure 4. Isobaric temperature dependences of magnetic moment μ, μ_B with inverse susceptibility χ^{-1}, magnetization σ, μ_B in orthorhombic state in the field with induction $B = 1$ T. Figures *5–15* specify pressure in kbar (*b*); pressure for μ and χ^{-1} in Figure 4, *a* increases from bottom to top from 5 to 15 kbar, μ, $\mu_B = 2sy$; σ, $\mu_B = 2sy\cos(\vartheta)$.

relationship between temperatures of magnetic transition T_C and structural transition T_t, consistency of their baric characteristics $\partial T_C/\partial P < 0$, $\partial T_t/\partial P > 0$ and abnormal inverse susceptibility form χ^{-1} near structural transition $(\partial\chi^{-1}/\partial T)_{T\le T_t} < 0$, $(\partial\chi^{-1}/\partial T)_{T\ge T_t} > 0$. Eventually, solutions of equations (1) provide theoretical dependences that adequately describe experimental results at atmospheric pressure, Figure 3.

At atmospheric pressure $(P = 0)$, temperature dependences of magnetization $\sigma[(\text{emu})/\text{g}] = M_0 y\cos(\vartheta)$ and inverse susceptibility $\chi^{-1} = H_0/(M_0 y)$ adequately describe the known facts of change in magnetic disordering behavior in MnAs from 1st order magnetostructural transitions FM(hex)–PM(orth) in low-induction fields $(B = 1\,\text{T})$ towards smooth isostructural magnetization decrease σ from a value in FM state to a value in magnetized PM state FM(hex) → PM(hex) in high-induction fields $(B = 10\,\text{T})$ [28]. $(M_0(x)$ is the saturation magnetization in local Mn spin model for a specimen with the specified x and spin s, which is calculated by $M_0[\text{emu/g}] = (1-x)2s\mu_B/A(x) = 1.116906s\,10000(1-x)/A(x)$, where $A(x)$ is the atomic weight per formula unit; $\chi^{-1}\,1T = 10000(M_0 y))$. For MnAs $x = 0$, $s = 2$.

When pressure rises higher than 5 kbar, no high-spin ferromagnetic hexagonal state HS FM(hex) occurs with crystal lattice (c1) $B8_1$. Theoretical dependences for cases $P \ge 5$ kbar and $B = 1$ T are shown in Figure 4. Curves in Figure 4, *a* show that the increase in structural PM transition temperature T_t with pressure growth correlates to the increase in magnetic moment μ and extension of the orthorhombic helicoidal order temperature range. In this case, isobaric temperature dependences of inverse paramagnetic susceptibility PM $\chi^{-1}(T)$ below the structural transition temperature T_t demonstrate baric abnormalities in the form of dependence peak $\chi^{-1}_{\text{orth}}(T)$. The review of the theoretical results has shown that the presence of such peak followed by dependence $\chi^{-1}_{\text{orth}}(T = \Theta_{\text{orth}})$ tending to zero with pressure increase was due to the fact that in elastic-structural dependence of Fourier components $J_i(Q_0^2, e_1)$ in (3b), $\lambda_{1i} < 0$ and $\lambda_i > 0$, $\lambda_{\text{ih}} > 0$. Dependences $\mu(T) = 2sy \equiv 4y$ at $T \le \Theta_{\text{orth}}$ describe near-spontaneous temperature behavior of a magnetic order parameter y in helimagnetic orthorhombic phase with crystal lattice B31. $\mu(T = 0,\ B = 0)$ describes spontaneous magnetic moment of orthorhombic phase and corresponds to low-spin state of MnAs. Isobaric temperature dependences of orthorhombic state magnetization $\sigma(T)$, $\mu_B = 2sy(T)\cos[\vartheta(T)] \equiv 4y\cos(\vartheta)$ in field $B = 1$ T behave less trivial than dependences $\mu(T)$ in this field. For curves $\sigma(T)$, peak at $T = T_m(P)$ is typical; in its turn, $\sigma(T_m)$ grows with pressure up to 11 kbar. Further pressure increase results in reduction of $\sigma(T_m)$, Figure 4, *b*. In Figure 5, theoretical and experimental temperature-magnetization dependences $\sigma(T)$ coincide when filed induction grows at a constant pressure of 11 kbar and 9 kbar, respectively.

Comparison of both curves suggests that the low-spin ferromagnetic state in MnAs in the orthorhombic phase is conditional.

In general, we can state that theoretical results describing the key baric features of MnAs may contribute to interpretation of some contradictory data [12,23] regarding high-pressure low-spin phases of MnAs.

3.2. $Mn_{1-x}Cr_xNiGe$ $(x = 0.11)$

For this germanide representative, dependences $v_0(e_1, e_2)$ and $J\big(q_a(Q_0^2, e_1)\big)$ shall provide some features common to germanides, which are discussed in the introduction. For details of selection of the applicable parameters of thermodynamic potential see [15–17]. Finally we obtain that a helicoidal structure HM(orth) with orthorhombic crystal lattice is a stable magnetic-ordered state at $P = 0$. This structure with wave vector $q[0, 0, q_a(x)]$ is easily distorted in a magnetic field and is accompanied with considerable magnetization in a relatively weak magnetic field. When field induction

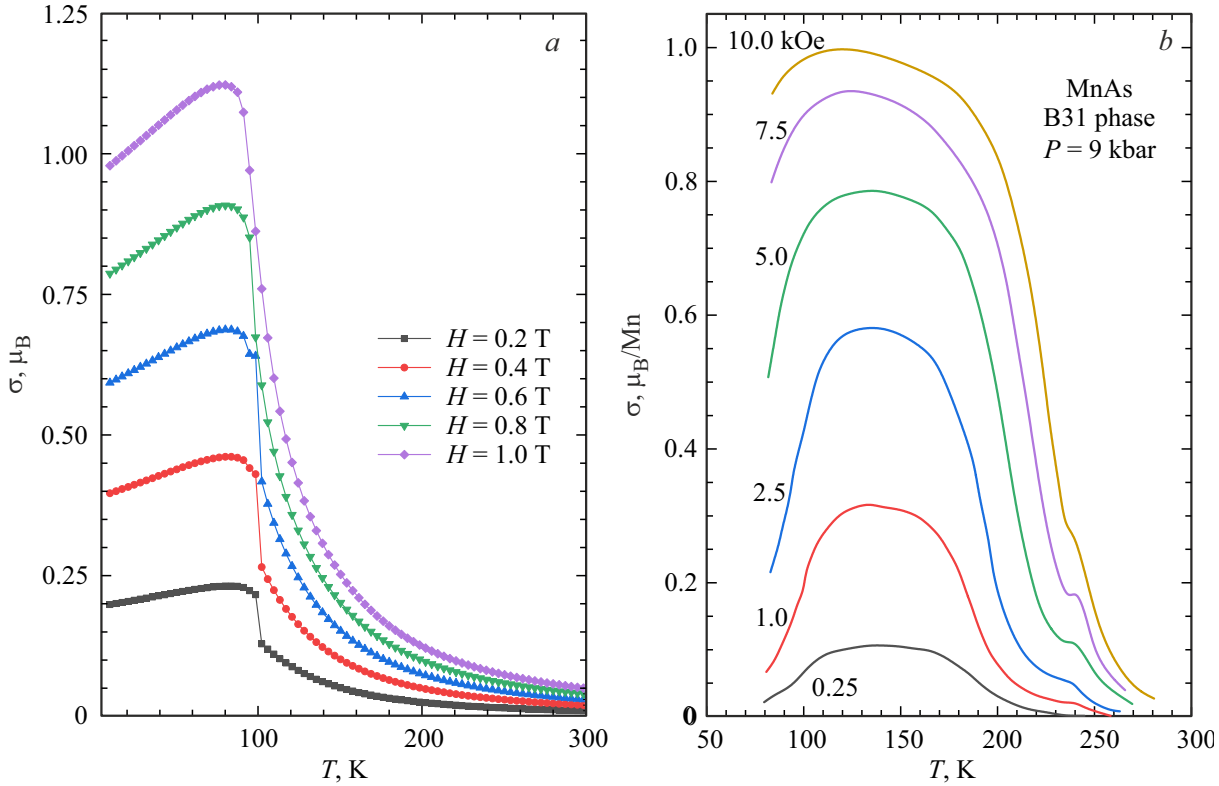

Figure 5. Aspects of change in temperature dependences of low-spin state magnetization of MnAs with change in the magnetic field. *a* — calculated dependences at $P = 11$ kbar; experimental data from [1] at $P = 9$ kbar.

increases, helimagnetic state HM(orth) is fully suppressed and magnetization increases up to maximum value 78 emu/g corresponding to ferromagnetism of orthorhombic phase FM(orth), Figure 6.

In Figure 6 $y_{\text{orth}} \equiv y(T, H_0, Q_0 \neq 0)$, $y_{\text{hex}} \equiv y(T, H_0, Q_0 = 0)$. The shown spontaneous dependences without field (a, b) and in field (c) adequately describe experimentally observed changes in magnetic characteristics of $Mn_{0.89}Cr_{0.11}NiGe$ at atmospheric pressure. In Figure 6, *a* the abnormal behavior of dependence $\chi^{-}(T)^{-1}$ typical of 1st order transition PM($Pnma$) $\leftrightarrow$ PM($P6_3/mmc$) (Figure 1, *b*) differs from the behavior of similar dependence in MnAs with 2nd order structural PM transition (Figure 1, *a*). This is achieved by the change of value and signs of applicable thermodynamic potential coefficients λ_i describing interrelation between structural order parameter Q_0 and magnetic order parameter y and coefficients L_2, L_3 taking into account connection between Q_0 and elastic deformations of lattice e_1 and orthorhombic distortions e_2. For germanide description, high values of L_2, L_3 are chosen at which structural transition PM(hex) $\leftrightarrow$ PM(orth) becomes 1st order transition and is accompanied with emergent changes $\chi^{-1}(T)$ of structural order parameter ΔQ_0 and elastic deformations Δe_1. In this case helimagnetic ordering at low temperatures T, due to relatively low λ_i, is implemented as 2nd order isostructural transition PM(orth) $\leftrightarrow$ HM(orth) without elastic deformation jumps and change in orthorhombic symmetry $Pnma$. In HM(orth) state, spontaneous magnetization of orthorhombic state is not available $(\cos(\vartheta) = 0)$, but occurs when the magnetic field increases, Figure 6, *c*. In firld $B = 5$ T, helimagnetizm is fully suppressed $(\cos(\vartheta) = 1)$ and helimagnetic orthorhombic state HM(orth) transforms to ferromagnetic orthorhombic state FM(orth), Figure 6, *c*. Ferromagnetic state with hexagonal lattice FM(hex), Figure 6, *a* for which paramagnetic Curie temperature is $\theta_{\text{hex}} < \theta_{\text{orth}}$ has a lower specific magnetic moment $\mu_{\text{hex}}^{\text{FM}} \approx 70$ emu/g $< \mu_{\text{orth}}^{\text{HM}} \approx 80$ emu/g and at is not implemented at $P = 0$. This is qualitatively agrees with experimental data [24,25] and, according to (11b), is due to the final value of orthogonal field $|\mathbf{O}_n^k| \equiv O(Q_0^2)$. At $|\mathbf{O}_n^k| \equiv 0$, according to (11b), magnetic moments in orthorhombic and hexagonal phases become the same even when $\theta_{\text{hex}} < \theta_{\text{orth}}$ at $T = 0$.

Under exposure to a pressure within 7–10 kbar, qualitative changes occur in temperature dependences of magnetostructural characteristics, Figure 7.

As shown in Figure 7, growth in hydrostatic pressure results in qualitative changes of magnetic ordering processes. At $P = 0$, when magnetic ordering temperature is considerably lower than structural transition temperatures $T_N \ll T_{t1} < T_{t2}$, magnetic ordering is implemented as 2nd order isostructural transition PM(orth) $\leftrightarrow$ HM(orth) with non-zero magnetization at low temperatures in a field with induction $B = 0.97$ T. At $P = 7$ kbar, when

$T_{t1} < T_N < T_{t2}$, isostructural magnetic ordering transforms into so called 1st order reversible magnetostructural transition PM(hex) → FM(orth). Where magnetic order at temperature decrease occurs at $T = T_{t1} < T_N$ and is accompanied with magnetization jumps Δ_1^σ of structural order parameter Δ_1^Q. In this case, as shown in Figure 7, *b*, helimagnetism is already suppressed in field $B = 0.97$ T ($\cos(\vartheta) = 1$ at $T \geq 0$). At reverse temperature increase, no jump-type processes are observed and magnetic disordering at $T_N < T_{t2}$ is implemented 2nd order as isostructural transition FM(orth) → PM(orth). At 14 kbar, dependence $\sigma(T)$, Figure 7, shows all attributes of full 1st order

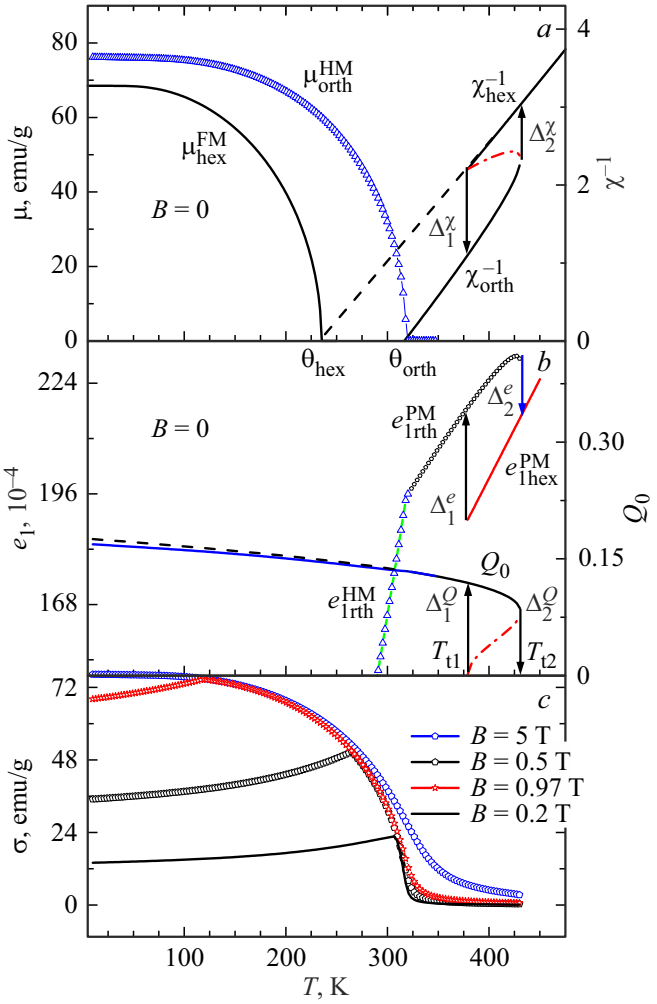

Figure 6. Theoretic dependences simulating temperature features of magnetostructural characteristics in $Mn_{0.89}Cr_{0.11}NiGe$ at $P = 0$. $\mu_{orth}^{HM} = y_{orth}M_0$ is the specific spontaneous magnetic moment ($B = 0$) of space-periodic orthorhombic helimagnetic state; χ^{-1} are inverse paramagnetic susceptibilities ($B = 0$); $\sigma = y_{orth}M_0\cos(\vartheta)$ is the specific spatially-homogeneous component of helimagnetic rhombic state (magnetization along magnetic fields with different induction B, T); vertical arrows show lability temperatures of hexagonal state T_{t1} and orthorhombic state T_{t2} in 1st order paramagnetic structural transition PM($Pnma$) ↔ PM($P6_3/mmc$); $\mu_{hex}^{FM} = y_{hex}M_0$ is the specific spontaneous magnetic moment of hexagonal FM state.

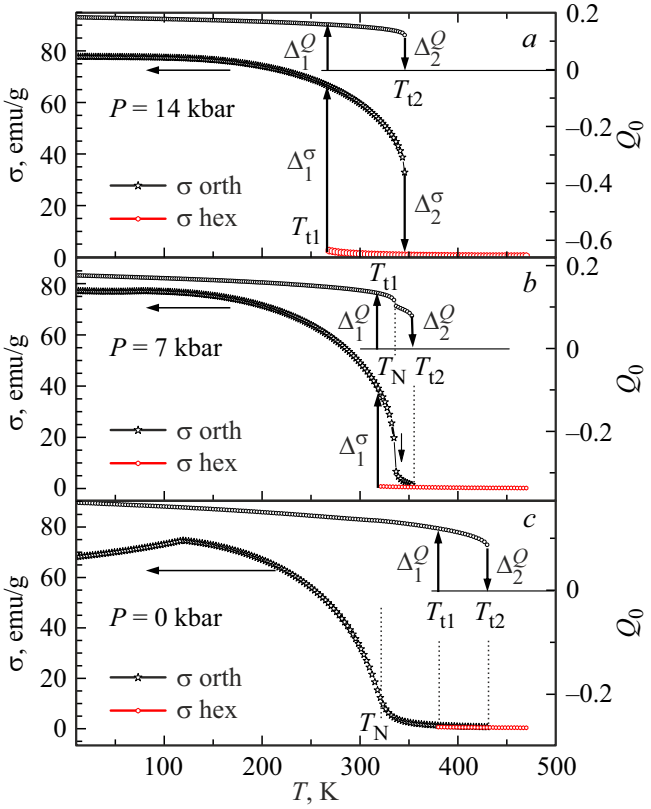

Figure 7. Theoretical temperature-magnetization dependences in field $B = 0.97$ T simulating qualitative changes of magnetic ordering processes in $Mn_{0.89}Cr_{0.11}NiGe$ under pressure.

magnetostructural transitions PM(hex) ↔ FM(orth) accompanied with jumps of magnetization $\Delta_{1,2}^\sigma$, structural order parameters $\Delta_{1,2}^Q$ and temperature histeresis $\Delta T = T_{t2} - T_{t1}$. These results are qualitatively agree with the experimental results [26] shown in Figure 8.

Review of the shown results discloses the baric change in magnetic phase transition behavior in a system with structural instability.

The change is based on possible partial (Figure 7, *b*) or full (Figure 7, *a*) coincidence of magnetic (T_N) and structural (T_t) instability temperatures under pressure. When the structural instability of a crystalline system is accompanied with jump-type processes in some $P-T$-region, then such coincidence leads to occurrence of jump-type processes in a spin subsystem with magnetic and structural order parameter interrelation. Subsequently, this leads to certain 1st order magnetostructural transitions in the whole system.

4. Features of magnetocaloric effect (MCE) in systems with structural transitions

The interest in the addressed systems is associated with MCE which becomes maximum near the temperatures of

1st order magnetostructural transitions at $0 \le P \le 2$ kbar for MnAs and at $P \ge 7$ kbar for $Mn_{0.89}Cr_{0.11}NiGe$. With some community of symmetry component of these transition, differences in magnetic-ordered phase symmetry become a decisive factor for MCE attenuation or enhancement by structural contribution. From general considerations, direct MCE in MnAs shall be attenuated by structural contribution in transition

$$\mathrm{FM}(\mathrm{hex}, Q_0 = 0,\ y > 0) \rightarrow \mathrm{PM}(\mathrm{orth}, Q_0 > 0,\ y = 0),$$

and in $Mn_{0.89}Cr_{0.11}NiGe$ in transition

$$\mathrm{HM}(\mathrm{orth}, Q_0 > 0,\ y > 0) \rightarrow \mathrm{PM}(\mathrm{hex}, Q_0 = 0,\ y = 0)$$

— it shall be enhanced. Actually, increase in magnetic entropy in MnAs, when magnetic order disappears ($y = 0$), is reduced due to structural order appearance ($Q_0 > 0$). In $Mn_{0.89}Cr_{0.11}NiGe$, magnetic disordering can be accompanied with disappearance of not only magnetic order ($y = 0$), but also structural order ($Q_0 = 0$), therefore both contributions enhance the general entropy increase. In Figure 9, isothermal entropy temperature dependences S in various magnetostructural states give

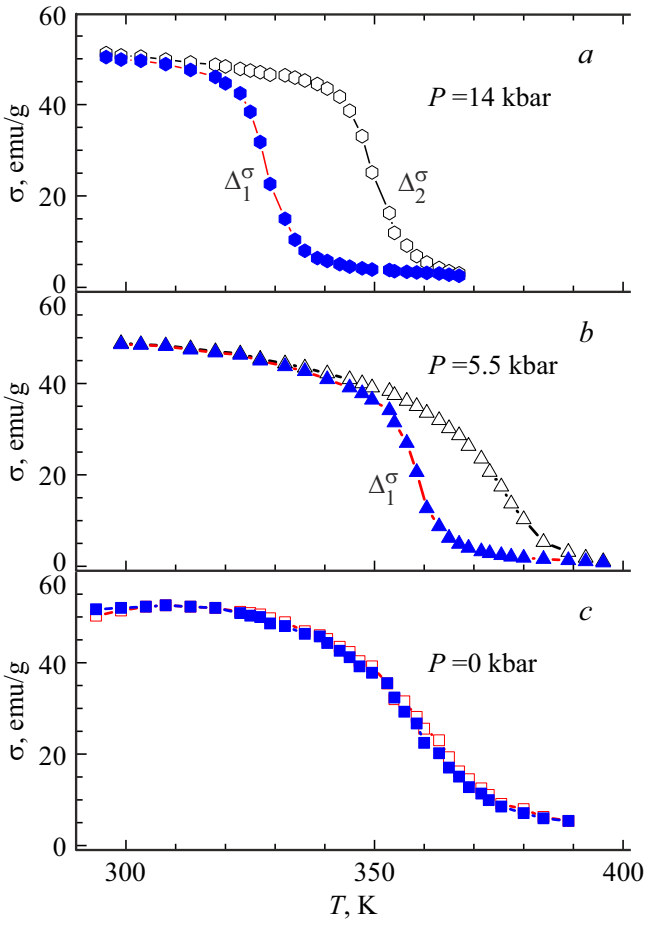

Figure 8. Dependences $\sigma(T)$ showing baric stimulation of 1st order magnetostructural transitions in $Mn_{0.89}Cr_{0.11}NiGe$. $\sigma(T)$ were measured in field $B = 0.97$ T [26].

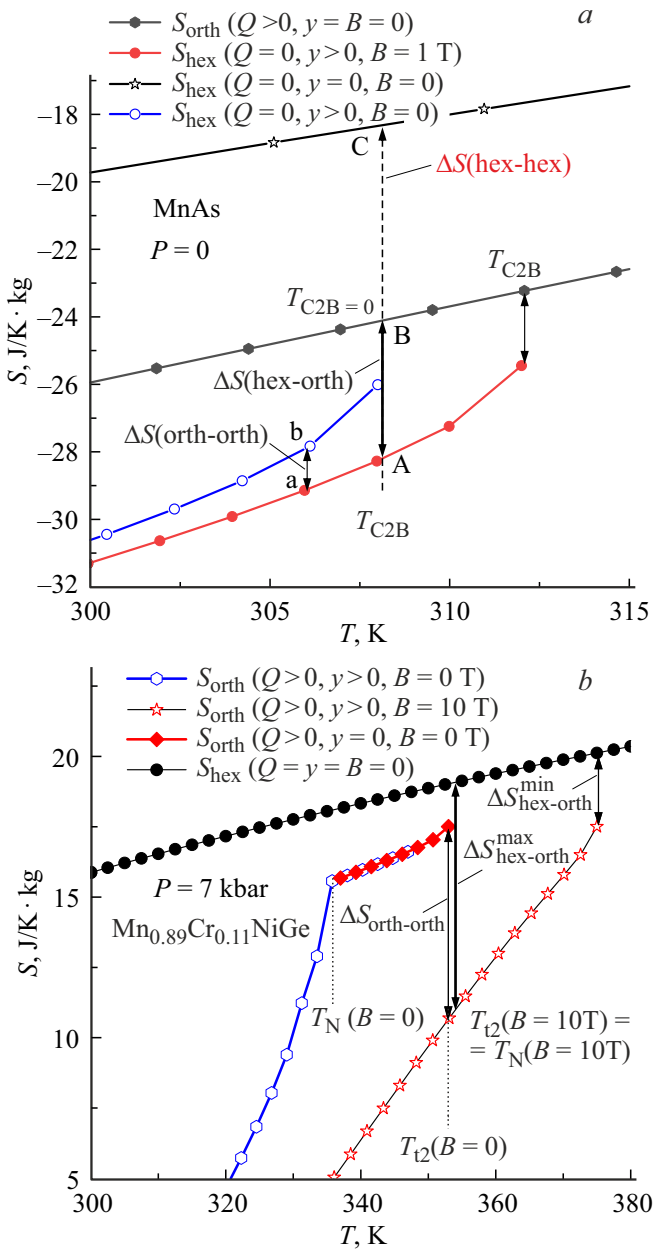

Figure 9. isothermal entropy temperature dependences in various magnetostructural states for MnAs ($P = 0$, $B = 1$ T) and $Mn_{0.89}Cr_{0.11}NiGe$ ($P = 7$ kbar, $B = 10$ T).

an idea of the structural contribution in MCE during demagnetization (field relief) below and above magnetic field disappearance temperatures T_{C2}, T_N in the addressed systems.

Based on MCE defined as difference ΔS between finite-field entropy of the system $S(B)$ and entropy $S(B = 0)$ at $B = 0$, proceed to the interpretation of various type of $\Delta S = S(B) - S(0)$ in Figure 9. As shown in Figure 9, *a*, demagnetization near $T \ge T_{C2}$ results in magnetostructural transition on line *AB*

$$\mathrm{FM}(\mathrm{hex}, Q_0 = 0,\ y > 0) \rightarrow \mathrm{PM}(\mathrm{orth},\ Q_0 > 0,\ y = 0)$$

and maximum absolute direct MCE

$$|\Delta S(\text{hex-orth})| = |S_{\text{hex}}(Q_0 = 0,\ y > 0,\ B = 1\,\text{T})$$

$$- S_{\text{orth}}(Q_0 > 0,\ y = B = 0)| = AB.$$

If finite state during demagnetization were hexagonal (point C on line $S_{\text{hex}}(Q_0 = y = B = 0)$), then this would result in an increase in absolute MCE value $|\Delta S(\text{hex-hex})| = AC > AB$. This hypothetical situation in MnAs illustrates a destructive role of structural contribution to MCE. Completely opposite situation in $Mn_{0.89}Cr_{0.11}NiGe$. As shown in Figure 9, *b*, demagnetization near $T \le T_{t2}(B = 0)$ results in magnetostructural transition

$$\text{HM}(\text{orth}, Q_0 > 0,\ y > 0) \rightarrow \text{PM}(\text{hex}, Q_0 = 0,\ y = 0)$$

and is accompanied with direct MCE

$$\Delta S(\text{hex-orth}) = S_{\text{orth}}(Q_0 > 0,\ y > 0,\ B = 10\,\text{T})$$

$$- S_{\text{hex}}(Q_0 = y = B = 0) < 0.$$

Demagnetization near $T \le T_{t2}(B = 0)$ results in isostructural transition

$$\text{HM}(\text{orth}, Q_0 > 0,\ y > 0) \rightarrow \text{PM}(\text{orth}, Q_0 = 0,\ y = 0),$$

which is accompanied here with considerable lower absolute MCE value

$$|\Delta S(\text{orth-orth})| = S_{\text{orth}}(Q_0 > 0,\ y = B = 0)$$

$$- S_{\text{orth}}(Q_0 > 0,\ y > 0,\ B = 10\,\text{T}) < |\Delta S(\text{hex-orth})|.$$

5. Conclusion

The discussed approach based on the uniform description of the displacement-type structural transition ($P6_3/mmc - Pnma$) helped to identify common and different features in the mechanisms that control baric components of magnetostructural and magnetocaloric properties in MnAs-based pnictides and MnNiGe-based germanides.

Funding

The study has been performed under the state assignment.

Conflict of interest

The authors declare that they have no conflict of interest.

References

[1] N. Menyuk, J.A. Kafalas, K. Dwight, J.B. Goodenough. Phys. Rev. **177**, 942 (1969).
[2] E.A. Zavadsky, V.I. Val'kov. Magnitnye fazovye perekhody. Nauk. dumka, Kiev, 1980) (in Russian).
[3] I.M. Vitebsky, V.I. Kamenev, D.A. Yablonsky. FTT **23** 215(1981). (in Russian).
[4] V.I. Val'kov, E.A. Zavadsky, B.M. Todris, S.K. Asadov. FTT **24**, 1531 (1982).
[5] J.S. Niziol, A. Zieba, R. Zach, M. Baj, L. Dmowski. J. Magn. Magn. Mater. **38**, 205 (1983).
[6] V.I. Val'kov, V.I. Kamenev, V.I. Mityuk, I.F. Gribanov, A.V. Golovchan, T.Yu. Delikatnaya. Phys. Solid State **59**, 274 (2017).
[7] V.I. Val.kov, I.F. Gribanov, B.M. Todris, A.V. Golovchan, V.I. Mitsiuk. Phys. Solid State **60**, 1125 (2018).
[8] I.F. Gribanov, V.V. Burkhovetsky, V.I. Val'kov, A.V. Golovchan, V.D. Zaporozhets, V.I. Kamenev. T.S. Sivachenko. FTVD **30**, *1*, 83 (2020).
[9] V.I. Val'kov, A.V. Golovchan, V.V. Koledov, V.I. Mityuk, I.F. Gribanov, V.D. Zaporozhets, B.M. Todris, T.S. Sivachenko. FTVD **29**, *3*, 5 (2019).
[10] R. Duraj, A. Deptuch, A. Szytuła, B. Penc, S. Baran. http://arxiv.org/abs/2207.02570v1
[11] S. Haneda, N. Kazama, Y. Yamaguchi, H. Watanabe. Phys. Sos. Jpn. **42**, 31 (1977).
[12] V.P. Glazkov, D.P. Kozlenko, K.M. Podurets, B.N. Savenko, V.A. Somenkov, Kristallografiya **48**, 59 (2003) (in Russian).
[13] Yu.S. Koshkid'ko, E.T. Dilmieva, J. Cwik, K. Rogacki, A.P. Kamantsev, V.V. Koledov, A.V. Mashirov, V.G. Shavrov, V.I. Valkov, A.V. Golovchan, A.P. Sivachenko, S.N. Shevyrtalov, V.V. Rodionova, V. Sampath. J. Alloys Compd. **798**, 810 (2019).
[14] A.P. Sivachenko, V.I. Mityuk, V.I. Kamenev, A.V. Golovchan, V.I. Val.kov, I.F. Gribanov. Low Temperature Physics **39**, 1051 (2013).
[15] V.I. Val.kov, A.V. Golovchan, V.V. Koledov, B.M. Todris, V.I. Mitsiuk. Phys. Solid State **62**, 798 (2020).
[16] V.I. Mitsiuk, G.S. Rimskiy, V.V. Koledov, A.V. Mashirov, V.I. Val'kov, A.V. Golovchan, O.E. Kovalev. Phys. Solid State **64**, *14*, 2310 (2022).
[17] V.I. Mityuk, G.S. Rimskiy, V.V. Koledov, A.V. Mashirov, V.I. Val'kov, A.V. Golovchan, O.E. Kovalev, B.M. Todris. Vesn. FFI № 3, C. 18 (2022) (in Russian).
[18] H.W.L. Alves. Phys. Status Solidi B **246**, 558 (2009).
[19] J. Lazewski, P. Piekarz, J. Tobola et al. Phys. Rev. Lett. **104**, 147205 (2009).
[20] J. Lazewski, P. Piekarz, K. Parlinski. Phys. Rev. B **83**, 054108 (2011).
[21] V.I. Val'kov, A.V. Golovchan. FTN **31**, *6*, 695 (2005) (in Russian).
[22] R. Blints, B. Zheksh. Segnetoelektriki i antisegnetoelektriki. Dinamika reshetki. Mir, M. (1975) (in Russian).
[23] I.F. Gribanov, E.A. Zavadsky, A.P. Sivachenko. FNT **5**, 1220 (1979) (in Russian).
[24] N.V. Mushnikov. UFN **182**, 450 (2012) (in Russian).
[25] J.-T. Wang, D.-S. Wang, C. Chen, O. Nashima, T. Kanomata, H. Mizuseki, Y. Kawazoe. Appl. Phys. Lett. **89**, 262504 (2006).
[26] V.I. Val.kov, V.I. Kamenev, A.V. Golovchan, I.F. Gribanov, V.V. Koledov, V.G. Shavrov, V.I. Mitsiuk, P. Duda. Phys. Solid State **63**, 1889 (2021).

Translated by Ego Translating